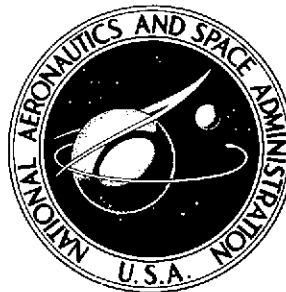2 mi4

NASA TECHNICAL NOTE

NASA TN D-7575

PERFORMANCE OF AN ASYMMETRIC SHORT ANNULAR DIFFUSER WITH A NONDIVERGING INNER WALL USING SUCTION

by *Albert* *J.* *Juhasz*

Lewis *Research* *Center*

Cleveland, *Ohio* *44135*

1. Report No. NASA TN D-7575	2. Government Accession No.	3. Recipient's Catalog No.
4. Title and Subtitle PERFORMANCE OF AN ASYMMETRIC SHORT ANNULAR DIFFUSER WITH A NONDIVERGING INNER WALL USING SUCTION		5. Report Date March 1974
		6. Performing Organization Code
7. Author(s) Albert J. Juhasz		8. Performing Organization Report No. E-7615
9. Performing Organization Name and Address Lewis Research Center National Aeronautics and Space Administration Cleveland, Ohio 44135		10. Work Unit No. 501-24
		11. Contract or Grant No.
12. Sponsoring Agency Name and Address National Aeronautics and Space Administration Washington, D.C. 20546		13. Type of Report and Period Covered Technical Note
		14. Sponsoring Agency Code

15. Supplementary Notes

16. Abstract

The performance of a short highly asymmetric annular diffuser equipped with wall bleed (suction) capability was evaluated at nominal inlet Mach numbers of 0.188, 0.264, and 0.324 with the inlet pressure and temperature at near ambient values. The diffuser had an area ratio of 2.75 and a length- to inlet-height ratio of 1.6. Results show that the radial profiles of diffuser exit velocity could be controlled from a severely hub peaked to a slightly tip biased form by selective use of bleed. At the same time, other performance parameters were also improved. These results indicate the possible application of the diffuser bleed technique to control flow profiles to gas turbine combustors.

17. Key Words (Suggested by Author(s)) Combustor flow control Diffuser bleed	18. Distribution Statement Unclassified - unlimited Cat. 12		
19. Security Classif. (of this report) Unclassified	20. Security Classif. (of this page) Unclassified	21. No. of Pages 41	22. Price* $3.25

NASA-C-168 (Rev. 6-71)

PERFORMANCE OF AN ASYMMETRIC SHORT ANNULAR DIFFUSER WITH A

NONDIVERGING INNER WALL USING SUCTION

by Albert J. Juhasz

Lewis Research Center

SUMMARY

The performance of a short, highly asymmetric annular diffuser equipped with wall suction capability was evaluated at nominal inlet Mach numbers of 0.188, 0.264, and 0.324 with the inlet pressure and temperature held at near ambient values. The diffuser had an area ratio of 2.75 and a length- to inlet-height ratio of 1.6. The straight, nondiverging inner diffuser wall was formed by a cylindrical section of the same diameter as that of the inlet passage inner surface. This section was mounted downstream of the inlet passage in such a manner that a narrow circumferential gap was left between the two surfaces for the purpose of applying small amounts of inner wall suction. The outer diffuser wall was shaped in a form of a torus of quarter-circle cross section and it was provided with two stepped suction slots, continuous over the full circumference. The performance parameters that were determined included exit velocity profile shape, diffuser effectiveness, percent total pressure loss, and diffuser efficiency.

Test results indicate that by selective use of suction, the exit velocity radial profile could be altered from a severely hub peaked to a center symmetric or even a slightly tip biased shape. At the same time, significant improvements in all the other performance parameters were also obtained at suction rates of four to nine percent of diffuser flow.

This capability of altering radial profiles of exit velocity and simultaneously improving diffuser performance, in general, suggests that the diffuser bleed technique may be used to control inlet airflow distribution in gas turbine combustors. The advantage of a combustor equipped with diffuser wall bleed capability would be the possibility of performance optimization at each of several operating conditions. For example, the combustor efficiency at idle operation might be increased by establishing a more favorable fuel-air ratio (near stoichiometric) in the primary zone, because most of the airflow could be directed to bypass the primary zone at the idling condition. Increasing primary zone efficiency would decrease emissions of carbon monoxide and unburned hydrocarbons (an annoying problem around airports). The ability to control the primary zone airflow distribution would also lead to improved altitude relight capability, because of the reduced velocity in the vicinity of the fuel nozzles and ignitors.

INTRODUCTION

The purpose of this investigation was to evaluate the use of diffuser wall bleed in an effort to improve the performance of annular diffusers of the type used between the compressor and combustor of gas turbine aircraft engines. The primary function of such diffusers is to reduce the velocity of the air leaving the compressor from a Mach number range of approximately 0.25 to 0.40 down to a range of 0.05 to 0.10, in order to ensure efficient combustion at a low total pressure loss. A second diffuser function, proposed in reference 1, would be to provide the combustor with a radial airflow distribution which is optimum for the particular engine operating condition. However, because gas turbine aircraft engines are required to operate at a wide range of conditions, a fixed diffuser geometry would represent either a compromise between the various operating conditions or the optimum design for a given condition such as cruise. In the former case, optimum combustor performance would not be obtained at any operating condition; in the latter case combustor performance would drop sharply at off-design conditions. Variable geometry diffusers could possibly provide the correct airflow distribution at each engine operating condition. However, such diffusers may be quite complex, because of mechanical linkages and overlapping surfaces which would have to be remotely operated.

An alternate method of controlling combustor inlet airflow distribution which is especially suited for advanced high-temperature engines which require turbine cooling was proposed in reference 1. This method employs an asymmetric diffuser with a gradually diverging inner wall and a rapidly diverging outer wall as shown in figure 1. The diffuser is also provided with wall bleed (suction) capability. In the present report, the term "bleed" denotes a small fraction of the diffuser flow which is ducted to a region of lower pressure as would be done in engine applications. The term "suction" denotes ducting of this flow to a subatmospheric sink, as was done in this component study. At idle and altitude relight conditions (fig. 1(a)), no bleed would be used; consequently, the asymmetric geometry would cause the diffuser exit velocity profile to be hub peaked. A hub peaked combustor inlet airflow distribution would be desirable at idle and altitude relight conditions. With a hub peaked inlet velocity profile most of the airflow would bypass the primary zone of the combustor, thus raising the local fuel-air ratio and combustion efficiency at idle. Simultaneously, exhaust emissions of unburned hydrocarbon and carbon monoxide would be reduced. While NO_x levels would not be reduced, they are low enough at the idling conditions to be negligible. During altitude relight operation, the hub peaked airflow profile would permit a low-velocity recirculation zone to be established in the region of the fuel nozzles and ignitors and thus create the fuel-air ratio conditions necessary to improve the potential of low-pressure relight.

At takeoff and cruise operation application of bleed flow on the outer wall of the diffuser would permit the combustor inlet airflow profile to be changed to a form that is

considered optimum, such as a low-curvature, center-peaked profile. Depending on combustor geometry, a small amount of bleed from the inner wall may also be needed for more precise profile control. Since the amount of bleed flow removed through the diffuser walls appears to be compatible with turbine cooling and auxiliary drive requirements (5 to 10 percent), there would be practically no net penalty on engine cycle efficiency.

Most of the data of reference 1 were obtained with a short annular diffuser having a symmetric axial section of its flow passage. In an effort to obtain data trends with simulated asymmetric passages some tests were also made with a cylindrical splitter ring installed in the diffusing passage. This splitter divided the diffusing passage into two asymmetric half annuli, each having a cylindrical nondiverging wall and a rapidly diverging opposite wall. Results indicated that diffuser exit velocity profile could be controlled by using wall suction.

A better simulation of the proposed asymmetric annular diffuser with high divergence on its outer wall and low divergence on its inner wall, was tested in reference 2. The asymmetric flow passage was obtained by displacing the inner surface of the symmetric diffuser exit duct, used in reference 1, radially outward. Results showed good control of diffuser exit velocity profile when suction was applied on both the inner and the outer wall. With suction applied to the outer wall only, the diffuser exit velocity profile could not be continuously controlled from hub peaked to tip peaked forms. The reason for this reduction in velocity profile control capability was inner wall flow separation, which occurred at a critical outer wall suction rate of 2.8 percent.

The present investigation was conducted to determine whether such inner wall flow separation could be prevented or delayed by changing the asymmetry of the diffuser. Performance data were obtained for a highly asymmetric diffuser, with all of the flow deceleration occurring on its outer wall. The diffuser had an area ratio of 2.75 and a length- to inlet-height ratio of 1.6. The inlet passage flow area was 304 square centimeters (47.12 in.^{2}). The straight, nondiverging inner diffuser wall was formed by a cylindrical section of the same diameter as that of the inlet passage inner surface. This section was mounted downstream of the inlet passage in such a manner that a narrow circumferential gap was left between the two surfaces for the purpose of applying small amounts of inner wall suction. The outer diffuser wall was shaped in the form of a torus of quarter-circle cross section and it was provided with two stepped suction slots, continuous over the full circumference. Velocity profiles, diffuser effectiveness, and diffuser pressure drop data were obtained for nominal diffuser inlet Mach numbers of 0.188, 0.264, and 0.324 at suction rates of zero to 9.5 percent of total flow. The greater part of the diffuser performance data were obtained with suction applied to the outer wall only. To check whether local separation was occurring on the cylindrical, nondiverging, inner wall, a limited number of measurements were made with suction

also applied on the inner wall through the previously mentioned narrow circumferential gap at the diffuser throat. All testing was conducted with air at near ambient temperature and pressure.

SYMBOLS

A   area

AR   diffuser area ratio

B   bleed flow fraction of total flow rate

C_p specific heat at constant pressure

g_c dimensional constant

H   diffuser inlet passage height

h   specific enthalpy

L   diffuser length

M   average Mach number at an axial station

$\dot{m}$ mass flow rate

P   average pressure at an axial station

p   local pressure at a radial position

R   gas constant for air

r   wall contour radius

S   entropy

T   temperature

V   average velocity at an axial station

v   local velocity at a radial position

X   downstream distance

γ specific heat ratio

ϵ diffuser efficiency, eq. (5)

η diffuser effectiveness, eq. (3)

ρ density

Subscripts:

act   actual conditions

atm   atmospheric condition

b   bleed or suction station

id   ideal conditions

m   maximum

r   local value at a given radial position

s   isentropic condition

0   stagnation condition

1   diffuser inlet station

2   diffuser exit station

APPARATUS AND INSTRUMENTATION

Flow System

The investigation was conducted in the test facility described in reference 2. A schematic of the facility flow system is shown in figure 2(a). Air, at a pressure of approximately 100 newtons per square centimeter (145 psia) and at ambient temperature is supplied to the facility by a remotely located compressor station. This air feeds the three branches of the flow system.

The center branch (identified as "main air line") is the source of airflow through the test diffuser. The air flowing through this branch is metered by a square-edged orifice installed with flange taps according to ASME standards. The air is then throttled to near atmospheric pressure by a flow control valve before entering a mixing chamber from which it flows through the test diffuser. The air discharging from the diffuser is exhausted to the atmosphere through a noise absorbing duct.

The two other branches of the flow system supply the two air ejectors, which produce the required vacuum for the inner and outer wall diffuser bleed flows. The ejectors are designed for a supply air pressure of 68 newtons per square centimeter (100 psia) and are capable of producing absolute pressures down to 2.38 newtons per square centimeter (7.0 in. Hg).

The inner and outer diffuser wall bleed flows are also metered by square-edged orifices. These orifices are also installed with flange taps according to ASME specifica-

tions in the suction flow lines that connect the inner and outer diffuser wall bleed chambers to their respective ejector vacuum sinks.

Diffuser Test Apparatus

The apparatus used in this investigation was essentially that of reference 2, but for a few modifications. A cross-sectional sketch including pertinent dimensions is shown in figure 2(b). As in reference 2, the centerbody that forms the inner annular surface is cantilevered from support struts located 30 centimeters (12 in.) upstream of the diffuser inlet passage. This construction minimized the possibility of strut flow separation having an effect on inlet velocity profile. In order to change the symmetric annular exit passage (used in ref. 1) to an asymmetric passage, a concentric cylinder was mounted on the downstream portion of the centerbody, which displaced the exit inner surface radially outward so that it was flush with the inlet inner surface.

Diffuser Walls

The removable diffuser walls are positioned in the apparatus as shown in figure 2(b). The details of the stepped slot, quarter torus wall geometry are shown in figure 3 which represents an axial section through the annular flow passage. The stepped slot geometry permits drawing off the suction flow in a direction parallel to the wall streamlines. On the outer wall, the 0.050-centimeter (0.020 in.) slots are located at 20° and 40° of arc measured from the start of the diverging passage. The nondiverging inner surface is formed by mounting a concentric exit cylinder, also shown in figure 3, on the original exit inner wall. This cylinder is so positioned that a gap, approximately 0.025 centimeter (0.010 in.) wide is left between its upstream knife edge and the original inner surface. The purpose of this gap is to permit the option of applying small amounts of suction on the nondiverging inner wall in addition to any suction applied to the outer wall. The outer and inner suction chambers have a toroidal shape of quarter circle cross section. They are held in place by 12 equally spaced 1.50-centimeter- (0.622-in. -) inside-diameter pipe nipples. These short pipes also serve to duct the inner and outer bleed flows into the inner wall suction plenum and the outer wall suction manifold (fig. 2), respectively.

The degree of asymmetry of this diffuser can be determined by considering the imaginary cylinder generated by rotating the centerline of the inlet passage about the rig centerline as a boundary between an outer and inner diffusing passage. The exit- to inlet-area ratio for the two passages can then be compared. For this diffuser, the outer pas-

6

sage has an area ratio of 4.34, while the inner passage area ratio is 1.00; that is, it is nondiffusing. The overall area ratio for the diffuser is 2.75 and the diffuser-length to inlet-height ratio is 1.6.

Diffuser Instrumentation

The essential diffuser instrumenation is indicated in figures 2 and 3. Diffuser inlet total pressure was obtained from three five-point total pressure rakes equally spaced around the annular circumference. Inlet static pressure was measured using wall taps in the vicinity of the inlet rakes.

Diffuser exit total and static pressures were obtained by using three nine-point pitot static rakes that could be rotated in a circumferential direction and translated axially. For this investigation these rakes were positioned a distance equal to twice the inlet passage height from the start of the diffusing section. Because the exit rakes had been designed for the larger exit passage of reference 1, they were mounted in the exit annulus in a position inclined to the axial plane. Thus each of the three exit rakes was measuring a diagonal profile over a 20° sector. All rake pressures were measured using three Scanivalves, each ducting pressures from a maximum of 48 ports to a flush mounted ± 0.69-newton-per-square-centimeter (± 1.0-psid) strain gage transducer. The valve dwell time at each port was 0.2 second, or over three times the interval required to reach steady state. Continuous calibration of the Scanivalve system was provided by ducting known pressures to several ports. Visual display of pressure profiles was made available by also connecting all inlet rakes and two exit rakes to common well manometers. The manometer fluid was dibutyl phthalate (specific gravity, 1.04).

All other pressure data such as orifice line pressures for the main air line and the subatmospheric bleed-air lines were obtained by use of individual strain gage pressure transducers. The temperatures of the various flows were measured with copper constantan thermocouples.

All data were remotely recorded on magnetic tape for subsequent processing with a digital data reduction program. In addition any test parameter could be displayed in the facility control room by means of a digital voltmeter.

PROCEDURE

Performance Calculations

Using the digital data reduction program mentioned previously, the overall diffuser performance was evaluated in terms of the radial profile of exit velocity, diffuser

effectiveness, total pressure loss, and diffuser efficiency. The values of the latter three figures of merit were expressed in percentages.

Intermediate computations included average static and total pressures, local and average Mach numbers and local- to average-Mach number ratios; that is, the equivalent of the local- to average-velocity ratios. The average pressures and Mach numbers at the diffuser exit, P_2, P_{02}, and M_2, were computed by trapezoidal integration using area ratio weighed pressures at the various radial positions. At the diffuser inlet, straight arithmetic averages were computed. Local Mach numbers for each pitot tube were computed from the compressible flow relation

$$M_r = \sqrt{\frac{2}{\gamma - 1}\left[\left(\frac{p_0}{p}\right)^{(\gamma-1)/\gamma} - 1\right]} \tag{1}$$

where p_0 and p represent the measured local total and static pressures and γ represents the specific heat ratio, set equal to 1.4 for the near ambient conditions of this investigation.

Diffuser and bleed airflow rates were computed from the respective orifice pressures and temperatures. As a check on the arithmetically averaged inlet Mach number a mean effective inlet Mach number was also computed by iteration from inlet airflow rate, total pressure, temperature, and area data as shown hereinafter

$$M_1 = \frac{\dot{m}_1}{P_{01}A_1}\sqrt{\frac{RT_{01}}{\gamma g_c}}\left(1 + \frac{\gamma - 1}{2}M_1^2\right)^{(\gamma+1)/2(\gamma-1)} \tag{2}$$

The velocity ratios at each radial position, needed to generate velocity profiles, were obtained from the circumferential averages of the local- to average-Mach number ratios. A plotting routine was used to generate the velocity profiles by computer with output on microfilm.

Diffuser effectiveness was computed from the following relation:

$$\eta = \frac{P_2 - P_1}{(P_{01} - P_1)\left[1 - \left(\frac{1 - B}{AR}\right)^2\right]} \times 100 \tag{3}$$

Equation (3) is an approximation expressing the ratio of actual to ideal conversion of inlet dynamic pressure to exit static pressure for the case of compressible flows through a diffuser with wall bleed for $M_1 \leq 0.5$ and $AR \geq 2$. For the conditions of the present study the use of equation (3) introduced an approximation error of less than 0.6 percent. A derivation of equation (3) and its limitations is shown in appendix A.

The total pressure loss was defined as

$$\frac{\Delta P_0}{P_{01}} = \frac{P_{01} - P_{02}}{P_{01}} \times 100 \tag{4}$$

Diffuser efficiency was computed from the relation

$$\epsilon = \frac{\left(1 + \frac{\gamma - 1}{2} M_1^2\right)\left(\frac{P_{02}}{P_{01}}\right)^{(\gamma-1)/\gamma} - 1}{\frac{\gamma - 1}{2} M_1^2} \times 100 \tag{5}$$

Equation (5) was derived in reference 3 for the case where the diffuser exit velocity is negligible. This restriction can be removed from equation (5), as shown in appendix B, by making a minor change in the definition and subsequent derivation of the diffuser efficiency parameter. Hence equation (5), as used in this report, relates the total energy level available at the exit of a diffuser, to the upstream total energy level with the inlet static enthalpy being the reference.

Test Conditions

Typical diffuser inlet conditions were the following:

Total pressure, N/cm^2 abs (psia) . . . . 10.1 to 10.3 (14.6 to 14.9)
Static pressure, N/cm^2 abs (psia) . . . . 9.3 to 9.8 (13.5 to 14.3)
Temperature, K (^{O}F) . . . . 276 to 279 (36 to 42)
Mach number . . . . 0.186 to 0.326
Velocity, m/sec (ft/sec) . . . . 62 to 109 (205 to 358)
Reynolds number (based on inlet passage height). . . . . 2.27×10^5 to 3.86×10^5
Bleed rate, percent of total flow . . . . 0 to 9.5

The U.S. Customary system of units was used for primary measurements and calculations. Conversion to SI units (Système International d'Unités) is done for reporting purposes only. In making the conversion, consideration is given to implied accuracy, which may result in rounding off the values expressed in SI units.

RESULTS AND DISCUSSION

The performance of the asymmetric annular diffuser was evaluated in terms of radial profiles of velocity, diffuser effectiveness, total pressure loss, and diffuser efficiency for each of the three inlet Mach numbers (0.188, 0.266, and 0.326) tested, with wall suction rates ranging from 0 to 9.5 percent. The greater part of the performance data was obtained with suction applied to the outer wall only. However, a limited number of data points were also obtained with suction on both walls, for comparison purposes. A summary of typical performance data is given in table I.

Radial Profiles of Inlet and Exit Velocity

Since the range of suction rates available for testing was greatest at the lowest inlet Mach number, the greater part of the velocity profiles that are presented were obtained at the 0.188 inlet Mach number. However, to demonstrate the invariance of velocity profile shape with inlet Mach number at a given suction rate, a few profiles for the 0.325 Mach number are also shown.

The computer plots of inlet and exit velocity profiles obtained for the 0.188 inlet Mach number at various suction rates are shown in figure 4. These profiles represent the ratio of local velocity at a radial position to the area weighted average velocity as a function of radial span position. The local velocity at a radial position was obtained by taking the average of local velocities at three circumferential positions. The resulting profiles give a fair representation of the flow, since the computed velocity spread due to circumferential nonuniformity was only ±2 percent for the inlet profiles and about ±25 percent for the exit profiles. The latter value was verified during occasional circumferential surveys of the diffuser exit flow.

Figure 4(a) shows inlet and exit profiles for the case of no suction. The inlet velocity profile has a slight hub bias that is characteristic for flow in annular passages. Such annular passage profiles have been treated previously, as for example in reference 4. Although no velocities were measured in the inner and outer wall boundary layers, the

estimated boundary layer profiles are drawn as shown by the dashed portions of the inlet profile. The higher velocity gradient on the inner surface of the annulus which gives rise to the hub skewed profile is caused by the higher shear stress on the inner wall. The total (inner and outer) boundary layer inlet area blockage for this profile is approximately 0.05. Because the inlet velocity profile is determined by the geometry of the inlet annular passage, it remains unchanged for the various suction rates tested (figs. 4(b) to (h)).

The exit velocity profile shape, however, is significantly affected by wall suction. Thus, in figure 4(a) it is highly hub peaked, with the velocity at the 10 percent of span position being over 1.8 times average velocity. The peak velocity at the 30 percent of span position is about 2.1 times average. In figure 4(b), the profile has shifted towards the center of the annular passage with about 2.5 percent suction applied on the outer wall. The velocity at the 10 percent of span position is now less than 1.6 times average, and the peak velocity now at the 40 percent position, has been reduced to about 1.85 times average velocity. The process of profile peak shifting radially outward and some profile flattening continues when the outer wall suction rate is increased to 3.7 percent as shown in figure 4(c). At outer wall suction rates of 4.8 and 6.3 percent (figs. 4(d) and (e)) the profiles tend toward symmetry about the imaginary center cylinder of the exit passage. However, local separation and reattachment occurs at the inner wall. This causes some of the pitot static tubes at the 10 percent of span position to register zero or near-zero values of velocity, thus depressing the circumferentially averaged values for this position shown on the plots. The zero value of velocity ratio at the 90 percent of span position in figure 4(e) is caused by the high degree of flow curvature, with the streamlines following the outer wall contour. The effect of this curvature on measured values of total and static pressure will be discussed in the next section. At outer wall suction rates of 7.8 and 8.8 percent (figs. 4(f) and (g)) the profiles are approximately symmetric with a parabolic shape. Peak velocity values of approximately 1.6 times average occur at the 60-percent position. The flow is now definitely attached to the outer wall, with local pockets of flow separation occurring on the inner wall, as indicated by the low value of velocity ratio at the 10 percent of span position and confirmed by probing the flow with tufts. Figure 4(h) shows the profile obtained with a suction rate of 7.65 percent on the outer wall and a suction rate of 1.8 percent through the inner wall gap at the diffuser throat (see fig. 3). Again, the profile is symmetric and it has a parabolic shape, not much different from the profile shapes of figures 4(f) and (g). Local separation on the inner wall is reduced, however, as indicated by a circumferential survey of velocities at the 10 percent of span position. This reduction of local separation effects on the inner wall also leads to higher diffuser effectiveness and lower total pressure loss values, to be discussed in subsequent sections.

Some typical velocity profiles obtained with an inlet Mach number of 0.325 are shown in figure 5. The inlet profiles are identical to those of figure 4. The exit profiles

also bear a striking resemblance to those of figure 4 at comparable suction rates. Thus the "no suction" profiles of figures 4(a) and 5(a) are practically congruent within the limits of experimental accuracy. Similar agreement exists between the profiles of figures 4(c) and 5(b), both measured at a suction rate of approximately 3.7 percent. Finally, the profile of figure 5(c), obtained with 5.2 percent suction, has a shape approximately in between that of figure 4(d) and that of figure 4(e) with suction rates of 4.7 and 6.3 percent, respectively.

In summary, the data presented in figures 4 and 5 show that the severely hub peaked exit velocity profiles of an asymmetric annular diffuser can be made symmetric by using suction on the outer wall. Minor improvements in flow control can be obtained by an additional amount of suction on the inner wall. Furthermore, for the conditions investigated, the exit velocity profile shape does not vary with inlet Mach number as long as the suction rate is kept constant.

Radial Profiles of Total and Static Pressure

To complement the discussion of velocity profiles, a brief examination of some typical measured total and static pressure profiles, which were used to compute the velocity profiles, is of interest. The inlet total pressure profiles were slightly biased toward the hub with pressure values at the 90 percent of span position being about 1 percent below the average values given in table I. The inlet static pressure profiles were not measured on a regular basis. However, occasional surveys with a pitot static probe showed that the static pressure was constant across the inlet passage. This justified the use of wall static pressure measurements to compute inlet velocity profiles.

Typical exit pressure profiles for the case of no suction and for the case of high outer wall suction, both at $M_1 = 0.188$, are shown in figure 6. In this figure the ratios of local-average-total- and local-average-static-pressure to atmospheric pressure are plotted as a function of radial span position. Without suction (fig. 6(a)), the total pressure profile is highly hub peaked with complete separation occurring on the outer wall, as indicated by the subatmospheric total pressure values in the outer half of the exit passage. In contrast to the total pressure profile, the static pressure profile is nearly flat, but for a slight hub bias. The velocity profile computed from the pressure profiles of figure 6(a) was shown in figure 4(a). With 6.3 percent suction on the outer wall (fig. 6(b)), the total pressure profile has been considerably flattened with the original severely hub peaked shape transformed into one with a slight tip bias. The tip peaked static pressure profile is indicative of outer wall flow attachment. However, the relatively high degree of tip peaking is caused by the radially outward curvature of the flow field. As indicated in figure 7-37 of reference 5, the resulting high yaw angles on the pitot static

12

tubes lead to measured total and static pressures that are lower than actual, with the error in total pressure exceeding that for the static pressure. Thus, the measured value of static pressure can be equal to or even exceed the measured total pressure, as shown at the 90-percent position in figure 6(b). The resulting zero value of computed velocity ratio at this position, as was shown for the velocity profile of figure 4(e), therefore is not caused by outer wall separation as might be first suspected. On the contrary, it is indicative of a radially outward curving flow with complete outer wall attachment. As mentioned in the preceding section, this outer wall attachment was also verified by probing the flow with tufts.

Some additional remarks may be made regarding the pressure profiles. First, to avoid the measurement problems caused by flow curvature, either directional measurement devices should be used, or measurement with parallel pitot static tubes should only be made at positions far enough downstream where flow streamlines would be more in line with the measuring tubes. Also, it is interesting to note that the static pressures at the measuring station are slightly below atmospheric. This is a further indication of the negative error in pressure measurement. Because of this negative error the diffuser performance results reported in this study are highly conservative.

Diffuser Effectiveness

Diffuser effectiveness, as defined by equation (3), is a measure of actual to ideal static pressure recovery. The effect of suction rate on diffuser effectiveness η is shown in figure 7 for the three inlet Mach number test conditions of this test program. The open symbols denote data obtained with suction on the outer wall only, while the solid symbols represent the limited amount of data obtained with suction on both the outer and the inner wall. As shown by the solid correlating curve for outer wall suction data and its dashed upper branch for suction on both walls, diffuser effectiveness does not vary with inlet Mach number. This is to be expected since the exit velocity profile shapes, discussed previously, did not show any inlet Mach number dependence either.

Regarding the effect of suction rate on diffuser effectiveness, the following observations may be made. With suction on the outer wall only, η increases from about 27 percent without suction to about 65 percent with 4.7 percent suction. Because of local flow separation effects on the inner wall, η cannot be increased beyond the 65-percent plateau by applying additional outer wall suction (solid curve). When a small amount of inner wall suction, approximately 1.8 percent, is added, however, diffuser effectiveness can be raised to about 73 percent at a total suction rate of 9.5 percent, as indicated by the dashed curve. This improvement in diffuser effectiveness is due to the reduction of locally separated regions on the inner wall.

It is interesting to compare the diffuser effectiveness data of this study with those obtained with a diffuser of lower asymmetry, tested in reference 2. With outer wall suction only, the diffuser effectiveness determined in reference 2 increased from 37 percent without suction to 52 percent at a suction rate of 2.8 percent. At this point the flow started to separate from the inner wall before it had become completely attached to the outer wall. This resulted in an abrupt decrease in η, from about 52 to 45 percent. When the flow finally became attached to the outer wall at about 5.5 percent suction, diffuser effectiveness could not be raised above a plateau of 52.5 percent with outer wall suction only. Also, the peak effectiveness obtained with suction on both walls was about 67 percent. Thus the small change in diffuser geometry represented by the present configuration resulted in improved performance, with inner wall separation occurring at a higher outer wall suction rate and being confined to local areas instead of occurring over the full inner wall surface.

<div align="center">Diffuser Total Pressure Loss</div>

The decrease of diffuser total pressure loss with suction rate is shown in figure 8 for the three inlet Mach numbers tested. The data trends confirm the explanation of flow behavior deduced from exit velocity profile and diffuser effectiveness data, discussed previously. Thus, with outer wall suction only (solid curves with open data points), total pressure loss decreases for all three inlet Mach numbers until a suction rate of 4.7 percent is reached. At this point, local separation effects on the inner wall prevent further decrease of total pressure loss by applying additional outer wall suction only. However, with a small amount of suction applied on the inner wall also, a further reduction in total pressure loss may be obtained at each inlet Mach number tested, as indicated by the dashed curves. These additional decreases in total pressure loss can only be due to a reduction of local flow separation effects on the inner wall. It should be pointed out that the decrease of diffuser total pressure loss with increasing suction rate is due mainly to a reduction of diffuser wall separation loss. Decrease in diffuser mass flow rate, due to a small fraction of the flow being drawn off through the suction slots, accounts for only a minor portion of the overall reduction in total pressure loss. This can be verified by considering the top curve of figure 8. With no suction, the total pressure loss is 3.90 percent. At a suction rate of 4.7 percent, the total pressure loss is only about 2.5 percent. Hence there is a reduction in total pressure loss of 1.4 percent. Of this reduction, assuming pressure loss to be proportional to the square of the diffuser flow rate, the amount due to reduced mass flow rate is $3.9 \times [1.0 - (1.0 - 0.047)^2] = 0.35$ percent. Hence, only about one fourth of the overall reduction in total pressure loss is due to decreased diffuser mass flow rate while three fourths is due to decreased wall separation loss.

14

Diffuser Efficiency

The isentropic diffuser efficiency, as defined by equation (5), is a measure of the total energy recovery. The diffuser efficiency parameter was included in the data analysis because it provides additional information on diffuser performance which is not readily apparent from a consideration of the diffuser effectiveness and total pressure loss parameters only. Yet there exists a definite relation between diffuser efficiency and the other two parameters, as will be discussed in the following paragraphs.

Values of diffuser efficiency and diffuser effectiveness are shown in table I for each test reading. Diffuser efficiency values exceed those of diffuser effectiveness for the data points without suction, for which the flow was completely separated from the outer wall. However, the two values are seen to approach each other as the suction rate is increased and the flow gradually becomes attached to both the inner and outer walls of the diffuser. The reason for these data trends is inherent in the definition of the two parameters. Diffuser efficiency relates the total available energy of the flow downstream of the diffuser to the upstream total energy. Diffuser effectiveness, on the other hand, expresses the ratio of actual-to-ideal conversion of dynamic pressure to static pressure. For test conditions involving flow separation from the outer wall, the velocities will be high and the static pressures will be low over the hub portion of the diffuser exit passage. Since the major portion of exit total energy is in the form of dynamic pressure which is a function of the square of the exit velocity, the computed value of diffuser efficiency will exceed that of diffuser effectiveness by a wide margin. Conversely, at sufficiently high suction rates to ensure attachment of the flow to both walls, the exit passage will be filled and, consequently, the diffuser exit velocity will be reduced and uniform over the entire exit passage. At these conditions most of the exit total energy will be in the form of static pressure energy and the values of diffuser efficiency and diffuser effectiveness will be approximately the same as indicated by the data in table I. The relation between diffuser efficiency, as defined in equation (5), the total pressure loss is illustrated in figure 9. Data points from this investigation are also shown to indicate the fairly wide range of diffuser efficiency and total pressure loss results at each inlet Mach number which was obtained by varying the amount of wall suction. Because of this range in results, the suction-type diffuser used in this study can be said to perform like a variable geometry device. Contrasted to the performance data shown in figure 9, the performance of a fixed geometry diffuser without suction would be described by a single value of pressure loss or efficiency for a given inlet Mach number.

As expected the use of suction improves diffuser efficiency. The lowest efficiency values for the three inlet Mach numbers tested, connected by the lower dashed line, represent test results without suction. Similarly, the upper dashed line connects the highest efficiency values obtained at high suction rates. The near-zero slope of these

dashed lines indicates that diffuser efficiency is practically invariant with inlet Mach number for the Mach number range tested.

It may also be observed in figure 9 that, for the range of total pressure loss values encountered in this study, the diffuser efficiency is a linear function of total pressure loss with inlet Mach number as a parameter. Although this linear relation is not immediately obvious from a superficial examination of equation (5), the proof is simple, as shown in appendix B. Thus the straight line correlation of diffuser efficiency data with small values of total pressure loss, with the slope of the correlating line being determined by the inlet Mach number, arises from the definition of diffuser efficiency. The small deviations of data points from the lines representing the test Mach numbers of 0.188, 0.264, and 0.324 are due to minor fluctuations of the test Mach numbers about their nominal values.

Aside from showing the range of diffuser efficiency and total pressure loss results of this study, figure 9 is also useful in estimating total pressure loss for diffusers in general, as long as diffuser efficiency and inlet Mach number are known. Moreover, as was shown in a previous paragraph, since diffuser efficiency and diffuser effectiveness become approximately the same for an unseparated diffuser operating at low exit velocity, total pressure loss for certain diffusers may also be directly estimated from inlet Mach number and diffuser effectiveness data usually quoted in the literature.

APPLICABILITY OF RESULTS TO COMBUSTOR DESIGN

The purpose of this investigation was to evaluate the merits of using suction to control the exit velocity profile of a short, highly asymmetric annular diffuser. The data trends discussed in the previous sections demonstrate that the exit velocity profile may indeed be drastically altered and diffuser performance in general may be significantly improved by using suction. Certain performance gains were also demonstrated by changing the geometry of the asymmetric diffuser from that of reference 2. Thus it would appear that the asymmetric bleed diffuser-combustor concept is practical from a flow profile control standpoint.

Additional questions remain to be answered, however. For example, the effect of combustor blockage on diffuser exit (combustor inlet) velocity distribution needs to be determined. It is reasonable to assume, of course, that in addition to diffuser geometry, the shape of the combustor and its location in the diffuser exit passage will be important factors in determining how well diffuser bleed could be applied in gas turbine combustors. The asymmetric bleed diffuser-combustor concept also has to be evaluated under burning conditions, preferably in full annular combustor test rigs. In such hot test evaluation the method of fuel injection will be a significant factor. Combustors

using pressure atomizing fuel nozzles appear to be most compatible with asymmetric bleed diffusers. This is so, because the bypassing of a large fraction of the airflow around the primary zone during idle and altitude relight operation would not degrade fuel atomization. In swirl-can combustors of the type tested in references 6 and 7, on the other hand, the airflow distribution would have to be controlled much more closely. The reason for this is that the primary zone velocity cannot be decreased below the value necessary for reasonably good fuel atomization. Even with this constraint, however, it is reasonable to expect performance improvements by airflow distribution control comparable to those obtained in reference 7 by radial stating of fuel. Additional performance improvements may materialize if both the radial distribution of airflow and fuel flow are controlled simultaneously.

Finally, bleed flow management in an actual engine application must be evaluated to determine cycle constraints and potential penalties.

SUMMARY OF RESULTS

Velocity profile control tests were conducted on a short, highly asymmetric annular diffuser equipped with contour wall bleed (suction) capability. The results were as follows:

1. Without the use of suction, the exit velocity profile was highly hub peaked and the flow was completely separated from the outer wall.

2. The exit velocity profile became center peaked with about 4.7 percent suction applied on the outer wall.

3. At outer wall suction rates in excess of 5 percent, the exit velocity profiles were biased toward the outer wall and small regions of local separation appeared on the inner wall. The profiles were much less peaked than the "no suction" profile.

4. With suction applied to both walls (1.8 percent on inner wall and 5 to 8 percent on outer wall) the exit velocity profile was symmetric about the annular centerline owing to the elimination of the locally separated regions on the inner wall.

5. The exit velocity profile shape, with or without suction, was not affected by inlet Mach number in the range of 0.18 to 0.33.

6. The inlet velocity profile shape was not affected by suction rate or inlet Mach number in the range of 0.18 to 0.33.

7. Diffuser effectiveness (ratio of actual to ideal static pressure recovery) could be creased from 27 percent with no suction to between 70 and 73 percent with 1.8 percent inner wall and 5 to 8 percent outer wall suction.

8. The diffuser total pressure loss at an inlet Mach number of 0.323 could be reduced almost in half, from 3.9 percent of inlet total pressure with no suction to 2.1 percent, with 1.7 percent inner and 5.2 percent outer wall suction. Similar reductions in total pressure loss were obtained at the 0.188 and 0.264 inlet Mach number test conditions.

Lewis Research Center,
　　National Aeronautics and Space Administration,
　　　　Cleveland, Ohio, November 2, 1973,
　　　　　　501-24.

APPENDIX A

DERIVATION OF DIFFUSER EFFECTIVENESS EQUATION

A schematic diagram illustrating flow through a diffuser with wall bleed is shown in figure 10. If steady, one-dimensional, ideal flow is assumed, the continuity equation can be written between inlet station 1 and exit station 2 as

$$\dot{m}_1 - \dot{m}_b - \dot{m}_2 = 0 \tag{A1}$$

or

$$\rho_1 A_1 V_1 - \dot{m}_b - \rho_2 A_2 V_2 = 0 \tag{A2}$$

from which

$$V_2 = \frac{\rho_1 A_1 V_1 - \dot{m}_b}{\rho_2 A_2} \tag{A3}$$

Defining

$$B = \frac{\dot{m}_b}{\dot{m}_1} = \frac{\dot{m}_b}{\rho_1 A_1 V_1} \tag{A4}$$

equation (A3) may be written as

$$V_2 = \frac{\rho_1 A_1 V_1 (1 - B)}{\rho_2 A_2} \tag{A5}$$

The energy equation for this flow is

$$\dot{m}_1 \left(h_1 + \frac{V_1^2}{2g_c}\right) - \dot{m}_b \left(h_b + \frac{V_b^2}{2g_c}\right) - \dot{m}_2 \left(h_2 + \frac{V_2^2}{2g_c}\right) = 0 \tag{A6}$$

Since the flow is assumed to be ideal, the energy per unit mass flow rate is constant throughout the diffuser. Thus we may write

$$h_1 + \frac{V_1^2}{2g_c} \equiv h_b + \frac{V_b^2}{2g_c} \equiv h_2 + \frac{V_2^2}{2g_c} \tag{A7}$$

Using identity (A7) and dividing by $\dot{m}_1$ equation (A6) can be rewritten as

$$h_1 + \frac{V_1^2}{2g_c} = B\left(h_1 + \frac{V_1^2}{2g_c}\right) + (1 - B)\left(h_2 + \frac{V_2^2}{2g_c}\right) \tag{A8}$$

If we substitute for V_2 from equation (A5) and note that $A_2/A_1 = AR$, equation (A8) may be rewritten after simplification as

$$h_2 - h_1 = \frac{V_1^2}{2g_c}\left[1 - \left(\frac{\rho_1}{\rho_2}\right)^2 \left(\frac{1 - B}{AR}\right)^2\right] \tag{A9}$$

Since for isentropic compressible flow

$$h_2 - h_1 = \frac{\gamma}{\gamma - 1}\left(\frac{P_2}{\rho_2} - \frac{P_1}{\rho_1}\right) \tag{A10}$$

the following expression may be obtained from equation (A9) for the ideal static pressure rise for compressible flow:

$$P_2 - P_1 = \left(\frac{\gamma - 1}{\gamma}\right)\frac{\rho_1 V_1^2}{2g_c}\left[1 - \left(\frac{\rho_1}{\rho_2}\right)^2 \left(\frac{1 - B}{AR}\right)^2\right] + P_2\left(1 - \frac{\rho_1}{\rho_2}\right) \tag{A11}$$

While equation (A11) represents the exact expression for the compressible flow static pressure rise, it is cumbersome to use because of the iterative procedure required to determine the unknown terms P_2 and ρ_2. This problem may be overcome in most cases without introducing appreciable error by making the substitutions and approximations discussed hereinafter.

The inlet dynamic pressure for compressible flow may be written as

$$P_{01} - P_1 = \left(\frac{\gamma - 1}{\gamma}\right)\frac{\rho_1 V_1^2}{2g_c} + P_{01}\left(1 - \frac{\rho_1}{\rho_{01}}\right) \tag{A12}$$

Another form of equation (A12) is

$$P_{01}\frac{\rho_1}{\rho_{01}} - P_1 = \left(\frac{\gamma - 1}{\gamma}\right)\frac{\rho_1 V_1^2}{2g_c} \tag{A13}$$

and equation (A11) may be rewritten as

$$P_2\frac{\rho_1}{\rho_2} - P_1 = \left(\frac{\gamma - 1}{\gamma}\right)\frac{\rho_1 V_1^2}{2g_c}\left[1 - \left(\frac{\rho_1}{\rho_2}\right)^2\left(\frac{1 - B}{AR}\right)^2\right] \tag{A14}$$

Dividing equation (A14) by equation (A13) shows that

$$\frac{P_2\dfrac{\rho_1}{\rho_2} - P_1}{P_{01}\dfrac{\rho_1}{\rho_{01}} - P_1} = \left[1 - \left(\frac{\rho_1}{\rho_2}\right)^2\left(\frac{1 - B}{AR}\right)^2\right] \tag{A15}$$

Multiplying equation (A12) by the right side of equation (A15) yields

$$(P_{01} - P_1)\left[1 - \left(\frac{\rho_1}{\rho_2}\right)^2\left(\frac{1 - B}{AR}\right)^2\right] = \left[\frac{\gamma - 1}{\gamma}\frac{\rho_1 V_1^2}{2g_c} + P_{01}\left(1 - \frac{\rho_1}{\rho_{01}}\right)\right]\left[1 - \left(\frac{\rho_1}{\rho_2}\right)^2\left(\frac{1 - B}{AR}\right)^2\right] \tag{A16}$$

where the second term to be summed on the right side of equation (A16) has a magnitude of about 2.5 times the first for $M_1 = 0.5$ and $AR = 2$. Comparison of equations (A11) and (A16) shows that the first terms on the right side of each are identical. Furthermore, for $M_1 \leq 0.5$ and $AR \geq 2$ the following approximation may be made for the second terms with less than 1.6 percent positive error:

$$P_{01}\left(1 - \frac{\rho_1}{\rho_{01}}\right)\left[1 - \left(\frac{\rho_1}{\rho_2}\right)^2 \left(\frac{1 - B}{AR}\right)^2\right] \doteq P_2\left(1 - \frac{\rho_1}{\rho_2}\right) \tag{A17}$$

The approximation (A17) may be verified by using equation (A15) and the isentropic flow tables which show that, for the restrictions quoted previously, the following is true:

$$\frac{P_2\left(1 - \dfrac{\rho_1}{\rho_2}\right)}{P_{01}\left(1 - \dfrac{\rho_1}{\rho_{01}}\right)} = \frac{P_2 \dfrac{\rho_1}{\rho_2} - P_1}{P_{01} \dfrac{\rho_1}{\rho_{01}} - P_1} \equiv \left[1 - \left(\frac{\rho_1}{\rho_2}\right)^2 \left(\frac{1 - B}{AR}\right)^2\right] \tag{A18}$$

With the approximation (A17) equation (A16) becomes

$$(P_{01} - P_1)\left[1 - \left(\frac{\rho_1}{\rho_2}\right)^2 \left(\frac{1 - B}{AR}\right)^2\right]$$

$$\doteq \frac{\gamma - 1}{\gamma} \frac{\rho_1 V_1^2}{2g_c}\left[1 - \left(\frac{\rho_1}{\rho_2}\right)^2 \left(\frac{1 - B}{AR}\right)^2\right] + P_2\left(1 - \frac{\rho_1}{\rho_2}\right) \tag{A19}$$

where the second term on the right side of equation (A19) has a positive error of less than 1.6 percent for $M_1 \le 0.5$ and $AR \ge 2$. Since the second term on the right side is about 2.5 times larger than the first term, the overall error of equation (A19) will be about 0.7 times 1.6 percent, or less than 1.2 percent positive. Equation (A11) may now be written as

$$P_2 - P_1 = (P_{01} - P_1)\left[1 - \left(\frac{\rho_1}{\rho_2}\right)^2 \left(\frac{1 - B}{AR}\right)^2\right] \tag{A20}$$

and the error in approximation (A20) is also less than 1.2 percent positive for $M_1 \le 0.5$ and $AR \ge 2$. Neglecting the density ratio term permits equation (A20) to be rewritten as

$$P_2 - P_1 \doteq (P_{01} - P_1)\left[1 - \left(\frac{1 - B}{AR}\right)^2\right] \tag{A21}$$

The error in equation (A21) will be at most 4.5 percent negative for $M_1 \leq 0.5$ and $AR \gtrsim 2$. Thus for $M_1 = 0.5$ and $AR = 4$ the error in equation (A21) will be about 1 percent negative, while for $M_1 = 0.3$ and $AR = 3$ the error will be about 0.6 percent negative. Increasing AR or reducing M_1 will decrease the error below these values.

Defining diffuser effectiveness as

$$\eta = \frac{(P_2 - P_1)_{act}}{(P_2 - P_1)_{id}}$$

where the numerator represents the measured static pressure rise and the denominator can be replaced by the right side of equation (A21) with the limitations due to approximation error understood. Equation (A22) then becomes

$$\eta = \frac{P_2 - P_1}{(P_{01} - P_1)\left[1 - \left(\frac{1 - B}{AR}\right)^2\right]} \tag{A23}$$

with the approximation errors being identical, except for sign reversal, to those quoted for equation (A21). Equation (A23) is identical to equation (3) with the approximation error understood.

For the case of incompressible flow, equation (A23) can be written as

$$\eta = \frac{P_2 - P_1}{\dfrac{\rho_1 V_1^2}{2g_c}\left[1 - \left(\frac{1 - B}{AR}\right)^2\right]} \tag{A24}$$

For the case of no bleed equation (A24), of course, becomes

23

$$\eta = \frac{P_2 - P_1}{\dfrac{\rho_1 V_1^2}{2g_c}\left(1 - \dfrac{1}{AR^2}\right)} \tag{A25}$$

which is a form usually found in the literature.

APPENDIX B

DERIVATION OF DIFFUSER EFFICIENCY EQUATION

The compression process occurring in a diffuser is shown in the enthalpy-entropy diagram of figure 11. This diagram differs from that given in reference 3 in that the total and static enthalpies at the diffuser exit, denoted by points 02 and 2, respectively, are not assumed to be equal. In fact they are shown to differ by the exit kinetic energy $V_2^2/2g_c$.

The isentropic diffuser efficiency ϵ is defined as

$$\epsilon = \frac{h_{02s} - h_1}{h_{02} - h_1} = \frac{\Delta h_s}{\dfrac{V_1^2}{2g_c}} \tag{B1}$$

For the case of constant specific heat C_p

$$\epsilon = \frac{T_{02s} - T_1}{T_{02} - T_1} = \frac{\dfrac{T_{02s}}{T_1} - 1}{\dfrac{T_{02}}{T_1} - 1} \tag{B2}$$

Since

$$\frac{T_{02s}}{T_1} = \left(\frac{P_{02}}{P_1}\right)^{(\gamma-1)/\gamma}$$

and

$$\frac{T_{02}}{T_1} = \frac{T_{01}}{T_1} = 1 + \frac{\gamma - 1}{2} M_1^2$$

equation (B2) may be written as

$$\epsilon = \frac{\left(\dfrac{P_{02}}{P_1}\right)^{(\gamma-1)/\gamma} - 1}{\dfrac{\gamma-1}{2}M_1^2} = \frac{\left(\dfrac{P_{01}}{P_{01}}\right)^{(\gamma-1)/\gamma}\left(\dfrac{P_{02}}{P_1}\right)^{(\gamma-1)/\gamma} - 1}{\dfrac{\gamma-1}{2}M_1^2} \qquad \text{(B3)}$$

And since

$$\left(\frac{P_{01}}{P_1}\right)^{(\gamma-1)/\gamma} = \frac{T_{01}}{T_1} = 1 + \frac{\gamma-1}{2}M_1^2$$

the isentropic diffuser efficiency can be expressed in percentage values as

$$\epsilon = \frac{\left(1 + \dfrac{\gamma-1}{2}M_1^2\right)\left(\dfrac{P_{02}}{P_{01}}\right)^{(\gamma-1)/\gamma} - 1}{\dfrac{\gamma-1}{2}M_1^2} \times 100 \qquad \text{(B4)}$$

which is identical to equation (5).

To show the linear relation between ϵ and total pressure loss, equation (B4) can be recast in the following form:

$$\epsilon = \frac{\left(1 + \dfrac{\gamma-1}{2}M_1^2\right)\left(1 - \dfrac{\Delta P_0}{P_{01}}\right)^{(\gamma-1)/\gamma} - 1}{\dfrac{\gamma-1}{2}M_1^2} \qquad \text{(B5)}$$

Differentiating equation (B5) with respect to $\Delta P_0/P_{01}$ results in

$$\frac{d\epsilon}{d\left(\dfrac{\Delta P_0}{P_{01}}\right)} = -\frac{\dfrac{\gamma-1}{\gamma}\left(1 + \dfrac{\gamma-1}{2}M_1^2\right)}{\dfrac{\gamma-1}{2}M_1^2\left(1 - \dfrac{\Delta P_0}{P_{01}}\right)^{1/\gamma}} = -\frac{2}{\gamma}\frac{\left(1 + \dfrac{\gamma-1}{2}M_1^2\right)}{M_1^2\left(1 - \dfrac{\Delta P_0}{P_{01}}\right)^{1/\gamma}} \qquad \text{(B6)}$$

26

For small values of total pressure loss, say $\Delta P_0/P_{01} \lesssim 0.05$, the term

$$\left(1 - \frac{\Delta P_0}{P_{01}}\right)^{1/\gamma} \doteq 1$$

and equation (B6) becomes

$$\frac{d\epsilon}{d\left(\dfrac{\Delta P_0}{P_{01}}\right)} \doteq -\frac{2}{\gamma} \frac{\left(1 + \dfrac{\gamma - 1}{2} M_1^2\right)}{M_1^2} \tag{B7}$$

Equation (B7) shows that for $\Delta P_0/P_{01} \leq 0.05$, with γ constant, the slope $d\epsilon/d(\Delta P_0/P_{01})$ is a function of inlet Mach number only and becomes increasingly more negative as the inlet Mach number decreases. Thus the observations made with regard to figure 9 are confirmed.

REFERENCES

1. Juhasz, Albert J.; and Holdeman, James D.: Preliminary Investigation of Diffuser Wall Bleed to Control Combustor Inlet Airflow Distribution. NASA TN D-6435, 1971.

2. Juhasz, Albert J.: Control of Exit Velocity Profile of an Asymmetric Annular Diffuser Using Wall Suction. NASA TM X-2710, 1973.

3. Shapiro, Ascher H.: The Dynamics and Thermodynamics of Compressible Fluid Flow. Vol. I. Ronald Press Co., 1953, pp. 151-152.

4. Brighton, J. A.; and Jones, J. B.: Fully Developed Turbulent Flow in Annuli. J. Basic Eng., vol. 86, no. 4, Dec. 1964, pp. 835-844.

5. Holman, J. P.: Experimental Methods for Engineers. McGraw-Hill Book Co., Inc., 1966, pp. 218-221.

6. Niedzwiecki, Richard W.; Juhasz, Albert J.; and Anderson, David N.: Performance of a Swirl-Can Primary Combustor to Outlet Temperatures of 3600° F (2256 K). NASA TM X-52902, 1970.

7. Niedzwiecki, Richard W.; Trout, Arthur M.; and Mularz, Edward: Performance of a Swirl-Can Combustor at Idle Conditions. NASA TM X-2578, 1972.

TABLE I. - DIFFUSER PERFORMANCE DATA

(a) Data with outer wall suction only

| Reading	Diffuser inlet Mach number, M_1	Airflow rate kg/sec	Airflow rate lb/sec	Total inlet pressure N/cm²	Total inlet pressure psia	Static inlet pressure N/cm²	Static inlet pressure psia	Inlet total temperature K	Inlet total temperature °F	Suction rate, percent Inner wall	Suction rate, percent Outer wall	Exit profile peak position, percent of span	Exit profile peak value, v_m/V	Diffuser effectiveness, η, percent	Diffuser efficiency, ϵ, percent	Total pressure loss, $\Delta P_0/P_{01}$, percent
65	0.261	3.29	7.26	10.27	14.89	9.71	14.08	276	37	0	0	30	2.02	27	45.6	2.54
66	.262	3.30	7.27	10.27	14.89	9.71	14.08				0	↓	2.02	26.8	45.3	2.56
67	.262	3.28	7.23	10.22	14.82	9.67	14.02				2.03		1.89	41.1	56.5	2.04
68	.262	3.28	7.24	10.22	14.82	9.66	14.01				2.00		1.90	41.3	56.4	2.05
69	.265	3.31	7.29	10.19	14.77	9.62	13.95	↓	↓	↓	3.16	↓	1.88	54.9	63.2	1.78
70	.264	3.30	7.27	10.19	14.77	9.62	13.95	276	37	0	3.22	30	1.84	55.2	64.3	1.71
71	.268	3.31	7.29	10.18		9.61	13.94				3.67	40	1.77	58.7	65.0	1.69
72	.265	3.31	7.30	↓		9.61	13.94				3.58	40	1.74	59.1	65.4	1.67
73	.263	3.28	7.24			9.62	13.96				4.32	50	1.77	62.8	67.0	1.57
74	.263	3.29	7.25	↓	↓	9.62	13.95		↓	↓	4.48	50	1.70	63.3	68.0	1.53
75	.263	3.29	7.25	10.18	14.77			276	37	0	4.29	50	1.72	63.2	67.1	1.57
76	↓	3.28	7.24								4.43	50	1.74	63.8	68.2	1.52
77		3.28	7.24								5.46	50	1.74	64.0	66.7	1.57
78	↓	3.28	7.24	↓	↓						5.42	60	1.72	64.4	67.4	1.54
79	.264	3.30	7.28	10.19	14.78	9.62	13.96	↓	↓	↓	6.44	60	1.72	64.5	67.1	1.57
80	.264	3.30	7.28	10.19	14.78	9.62	13.95	276	37	0	6.45	60	1.72	64.1	66.5	1.60
83	.188	2.38	5.25	10.12	14.69	9.83	14.27		36		0	30	2.08	28.5	46.1	1.31
84	.188	2.38	5.24	10.12	14.68	9.84	14.26				0	30	2.04	28.4	46.3	1.31
85	.185	2.34	5.16	10.08	14.62	9.80	14.22		↓	↓	2.42	30	1.82	46.1	59.5	.96
86	.186	2.35	5.18	10.08	14.62	9.80	14.22	↓	↓		2.46	40	1.86	46.4	59.2	.98
87	.188	2.37	5.22	10.07	14.60	9.78	14.19	276	37	0	3.66	40	1.69	60.4	65.8	.83
88	.188	2.37	5.23		14.61	9.78	14.19				3.70	40	1.71	61.1	67.7	.80
89	.189	2.39	5.26				14.19				4.70	50	1.74	65.3	67.5	.81
90	.189	2.38	5.25	↓		↓	14.18				4.76	40	1.70	64.6	66.0	.84
91	.189	2.38	5.25	↓			14.19				6.31	60	1.68	64.4	65.5	.86
92	.189	2.38	5.25	10.07	14.61	9.78	14.19	276	37	0	6.37	60	1.69	64.3	65.2	.86
93	.189	↓	5.25								7.68		1.61	65.4	65.7	.85
94	.188	↓	5.24								7.82		1.67	65.4	65.5	.85
99	.189	↓	5.26								8.81	↓	1.61	65.3	64.7	.87
100	.188	2.37	5.22	↓	↓	↓	↓	↓	↓	↓	8.95		1.62	65.4	65.0	.86
101	.323	3.95	8.71	10.24	14.85	9.39	13.62	279	42	0	0	30	2.02	27.5	44.7	3.90
102	.323	3.95	8.71	10.24	14.85	9.39	13.62	279	42		0		2.05	27.6	44.5	3.91
103	.323	3.94	8.68	10.19	14.78	9.35	13.56	278	41		1.37		1.99	36.3	50.7	3.48
104	.324	3.95	8.70	10.18	14.77	9.34	13.55	278	41		1.38		1.97	36.9	52.3	3.40
105	.324	3.94	8.69	10.17	14.75	9.31	13.50	278	40	↓	2.05	↓	1.96	41.6	53.6	3.29
106	.325	3.95	8.71	10.16	14.74	9.31	13.50	278	40	0	2.04	30	1.95	41.6	55.1	3.20
107	.326	3.94	8.70	10.12	14.67	9.27	13.44				3.14	30	1.94	51.4	60.0	2.88
108	.326	3.95	8.70	10.12	14.67	9.27	13.44				3.10	30	1.95	51.4	59.8	2.89
109	.324	3.93	8.65	10.11	14.66	9.25	13.42				3.71	40	1.71	58.3	64.0	2.57
110	.324	3.93	8.65	10.11	14.66	9.25	13.42	↓	↓	↓	3.69	40	1.70	58.4	63.6	2.59
111	.325	3.93	8.67	10.11	14.66	9.25	13.42	278	40	0	4.13	50	1.68	61.8	65.1	2.50
112	.324	3.92	8.65		14.67	9.25	13.42				4.14	50	1.64	61.2	64.7	2.51
113	.325	3.94	8.68			9.25	13.41				4.60	60	1.66	62.6	66.2	2.43
114	.324	3.93	8.66	↓		9.24	13.41				4.63	50	1.71	62.6	64.7	2.52
115	.325	3.94	8.69	10.12		9.25	13.41				5.22	60	1.74	63.3	64.4	2.56
116	.326	3.95	8.70	10.11	↓	9.25	13.42	↓	↓	↓	5.20	60	1.68	63.4	65.7	2.47

TABLE I. - Concluded. DIFFUSER PERFORMANCE DATA

(b) Data with suction on both walls

Read-ing	Diffuser inlet Mach number, M_1	Airflow rate kg/sec	Airflow rate lb/sec	Total inlet pressure N/cm²	Total inlet pressure psia	Static inlet pressure N/cm²	Static inlet pressure psia	Inlet total temperature K	Inlet total temperature °F	Suction rate, percent Inner wall	Suction rate, percent Outer wall	Suction rate, percent Total	Exit profile peak position, percent of span	Exit profile peak value, v_n/V	Diffuser effectiveness, η, percent	Diffuser efficiency, ϵ, percent	Total pressure loss, $\Delta P_0/P_{01}$, percent
81	0.266	3.30	7.29	10.14	14.70	9.61	13.93	276	37	1.79	6.36	8.15	50	1.68	71.2	71.2	1.40
82	.266	2.39	7.27	10.13	14.70	9.60	13.93	↓	↓	1.78	6.35	8.12	60	1.66	71.2	71.4	1.38
95	.190	2.39	5.26	10.05	14.58	9.77	14.18			1.81	7.73	9.54	60	1.69	73.0	69.0	.77
96	.190	2.39	5.27	10.05	14.57	9.77	14.18			1.80	7.65	9.45	60	1.62	72.8	71.5	.72
97	.188	2.37	5.22	10.05	14.57	9.78	14.19	↓	↓	1.81	6.24	8.05	50	1.66	72.1	70.7	.72
98	.189	2.38	5.24	10.05	14.58	9.78	14.18	276	37	1.80	6.40	8.20	50	1.69	71.4	70.4	.73
117	.328	3.94	8.70	10.06	14.59	9.24	13.41	278	40	1.74	5.16	6.90	40	1.65	69.9	70.1	2.18
118	.329	3.96	8.72	10.06	14.59	9.24	13.40	278	40	1.71	5.21	6.93	40	1.62	70.3	71.2	2.12
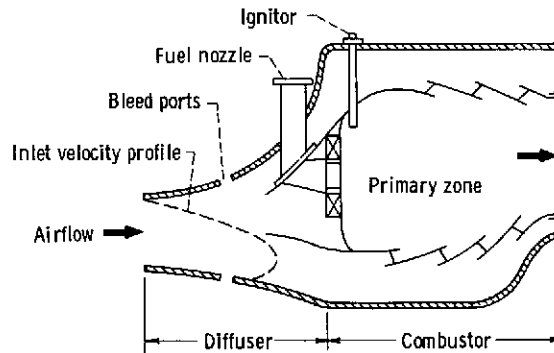
(a) Idle or altitude relight operation.
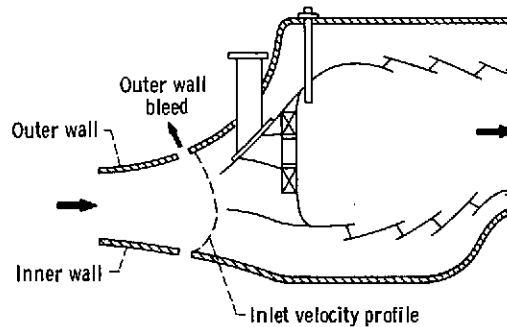
(b) Cruise or takeoff operation.

Figure 1. - Application of diffuser bleed in short annular asymmetric diffuser-combustor.
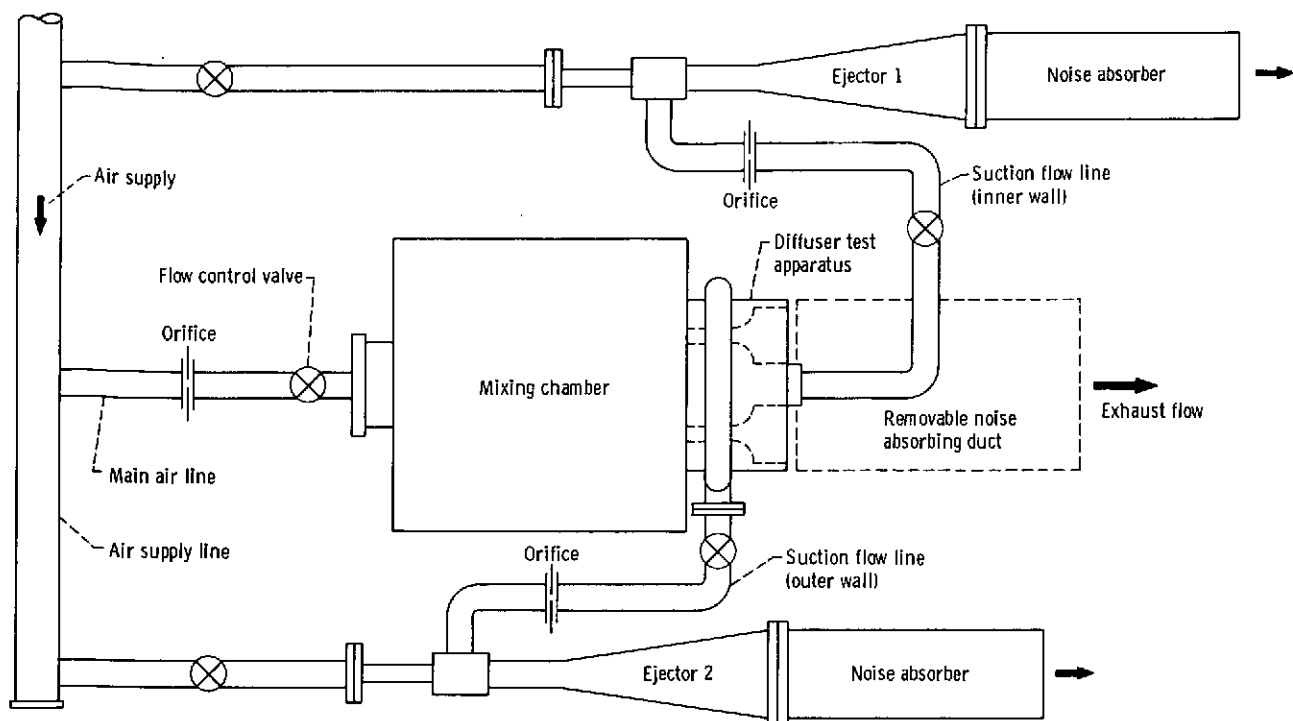
(a) Flow system.
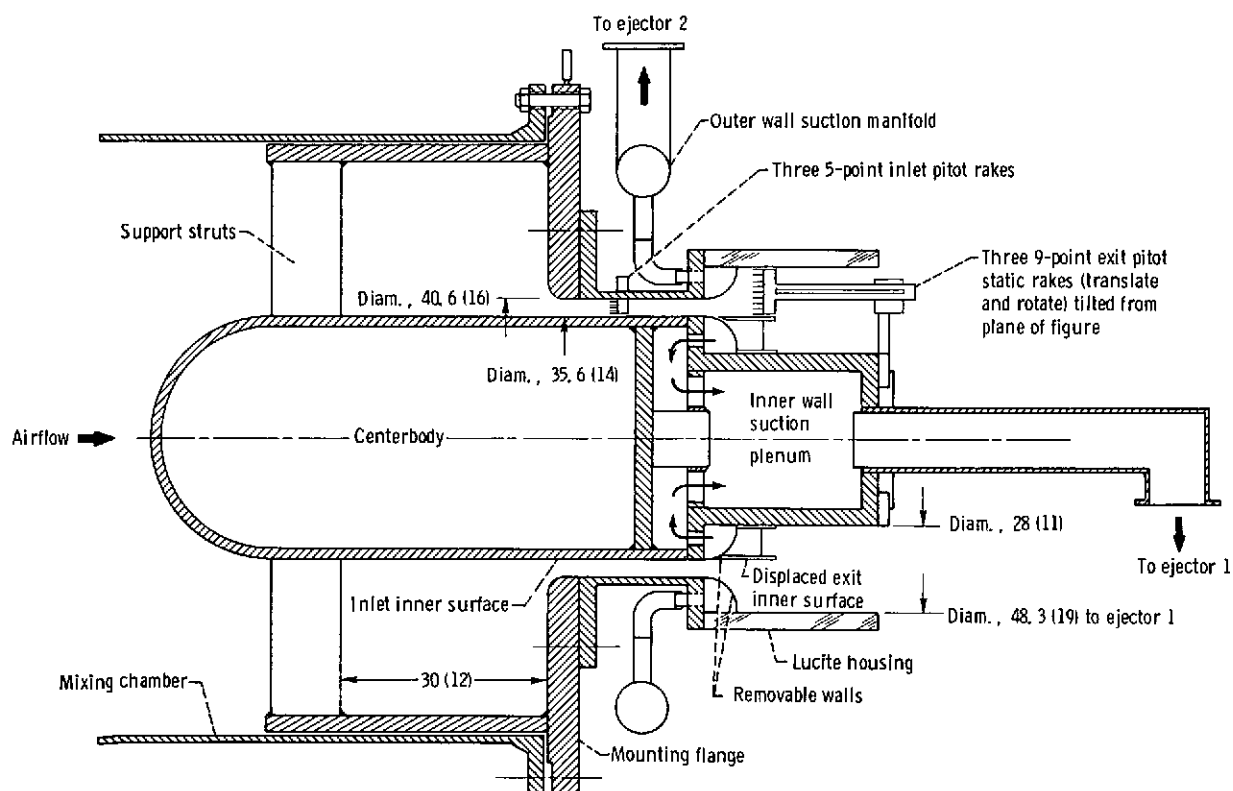
(b) Axial section of asymmetric annular diffuser test apparatus. (Dimensions are in cm (in.).)

Figure 2. - Test facility.
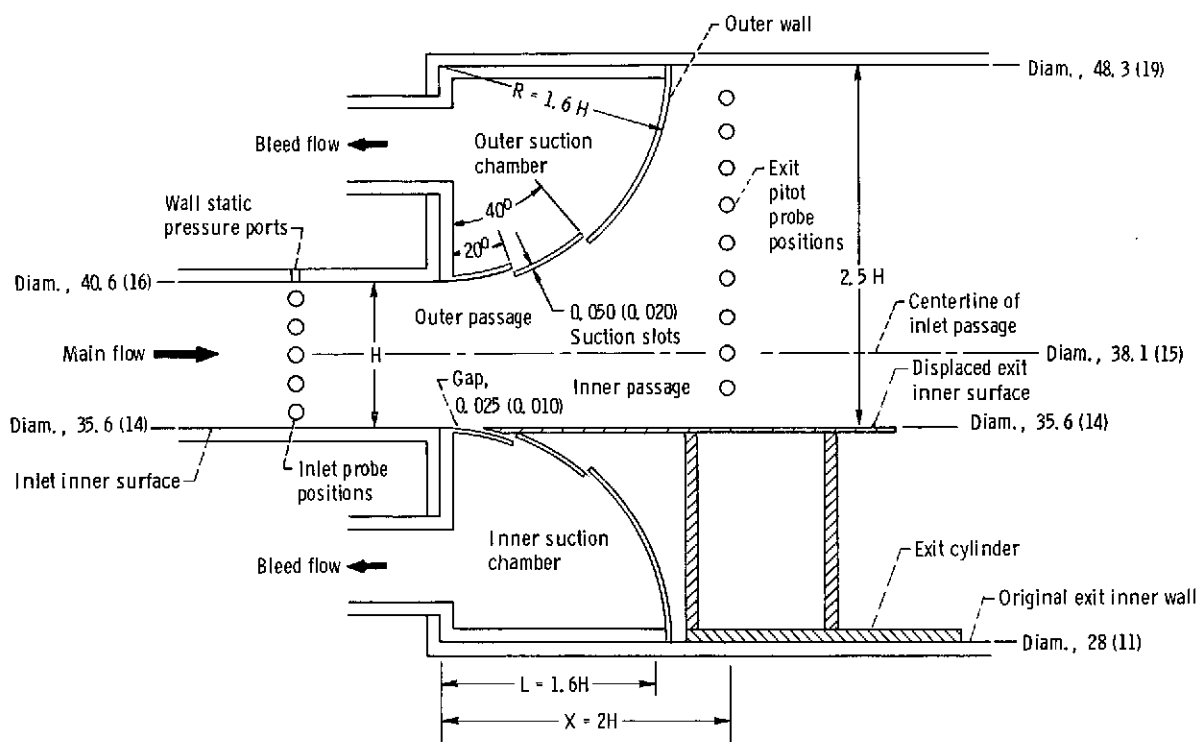
Figure 3. – Axial section through annular flow passage showing diffuser contour wall detail; inlet passage height, H, 2.54 cm (1.0 in.). (Dimensions are in cm (in.) unless indicated otherwise.)
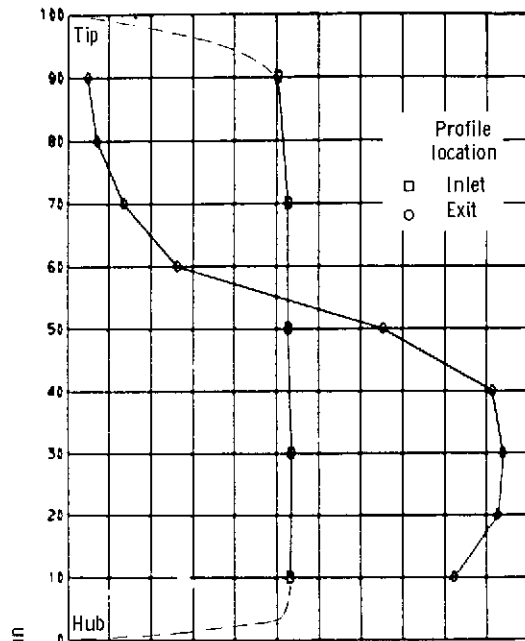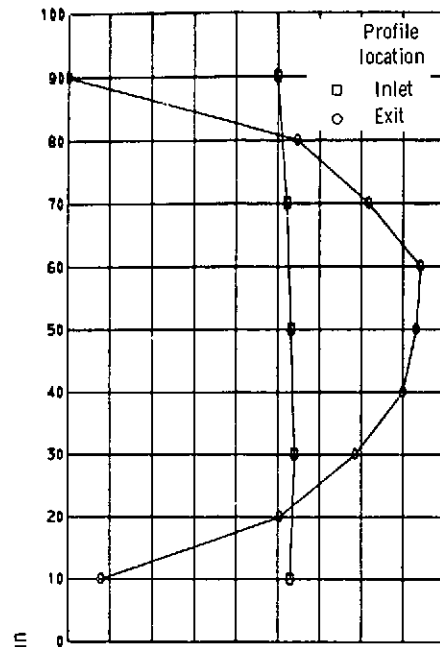
(a) No suction.
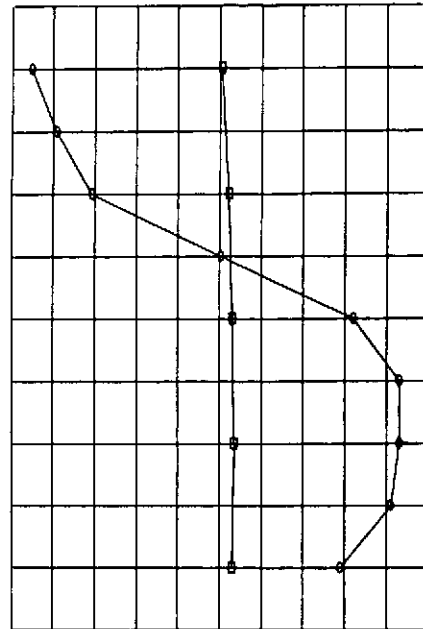
(b) Outer wall suction, 2.46 percent.
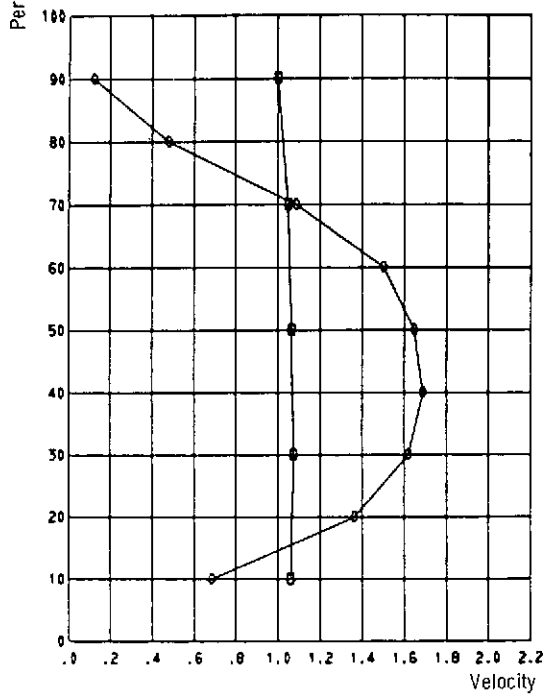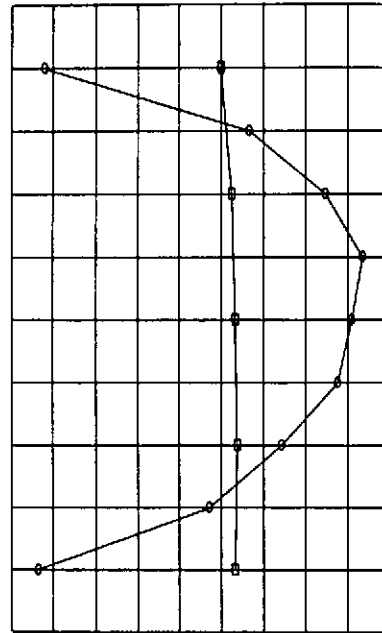
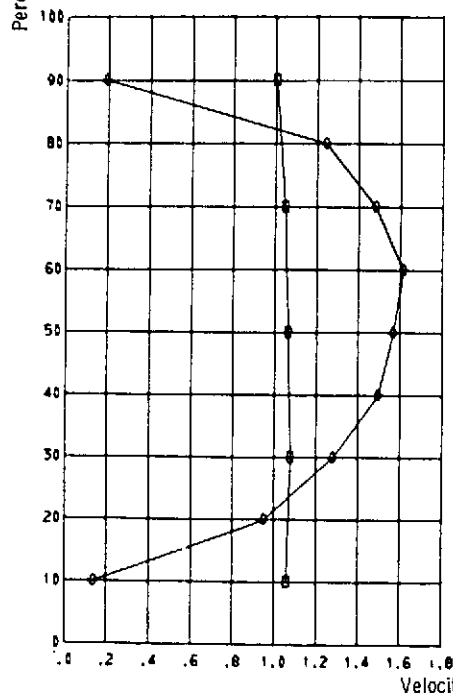(c) Outer wall suction, 3.66 percent.
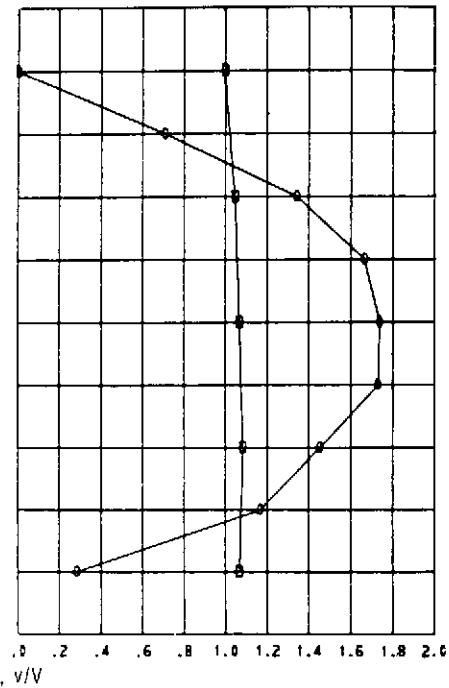
(d) Outer wall suction, 4.7 percent.

Figure 4. - Radial profiles of diffuser inlet and exit velocity at various suction rates. Diffuser inlet Mach number, 0.188.

(e) Outer wall suction, 6.3 percent.

(f) Outer wall suction, 7.82 percent.

(g) Outer wall suction, 8.8 percent.
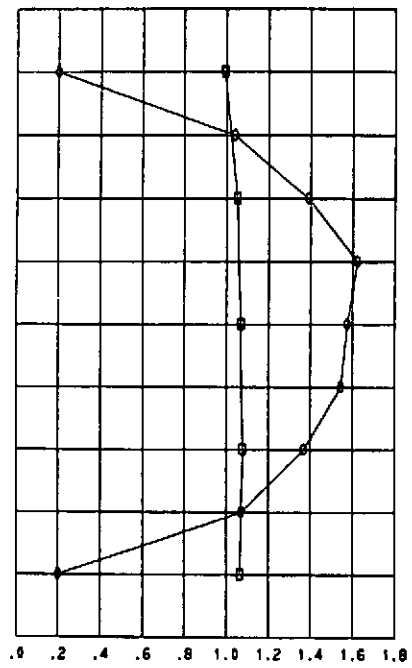
(h) Inner wall suction, 1.8 percent; outer wall suction, 7.65 percent.

Figure 4. – Concluded.
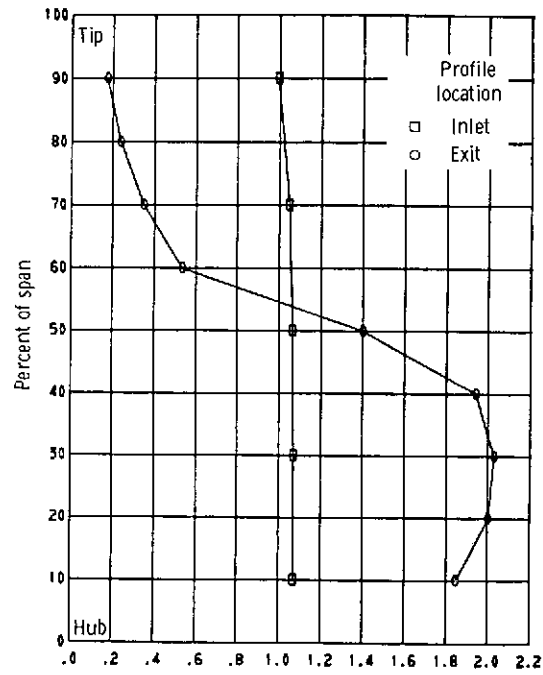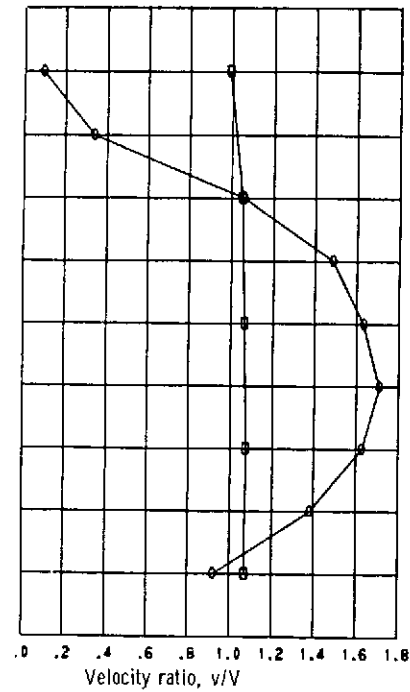
(a) No suction. (b) Outer wall suction, 3.71 percent. (c) Outer wall suction, 5.22 percent.
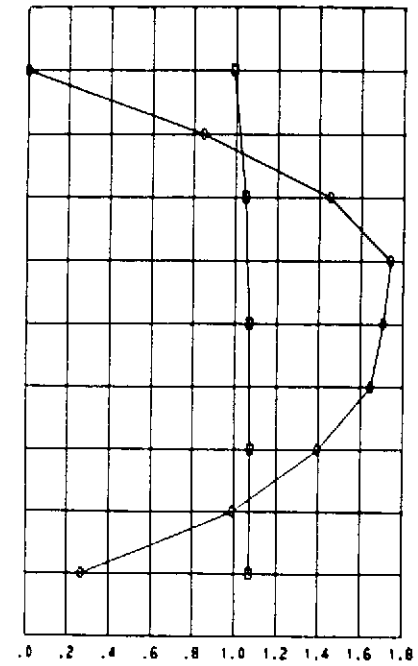
Figure 5. - Radial profiles of diffuser inlet and exit velocity at various suction rates. Diffuser inlet Mach number, 0.325.

(a) No suction.

(b) 6. 3 Percent outer wall suction.
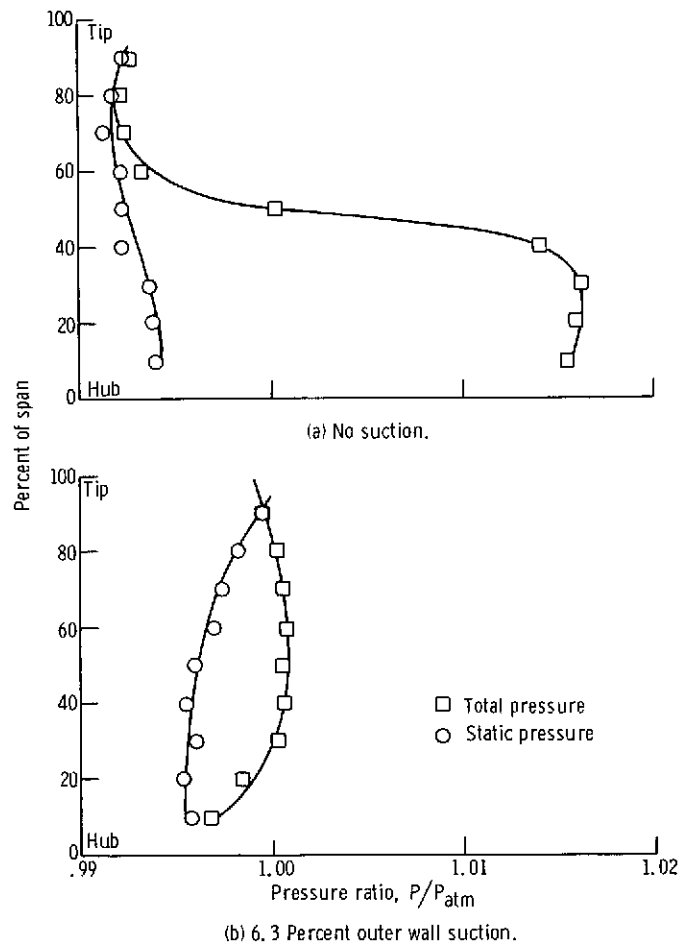
Figure 6. - Measured total and static pressure profiles at diffuser
exit for diffuser inlet Mach number of 0. 188.
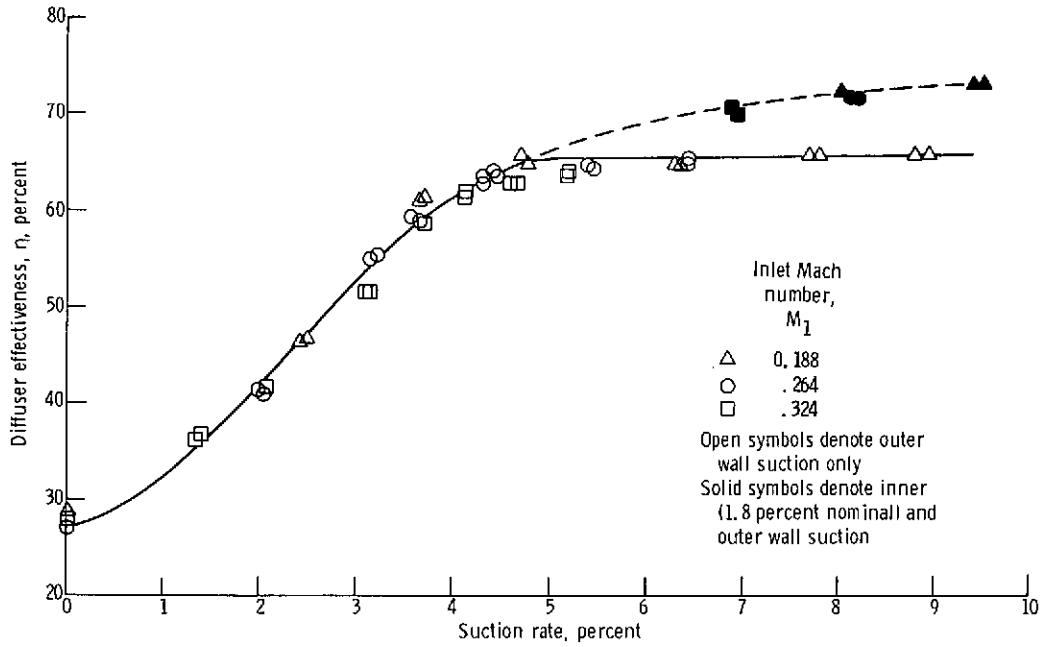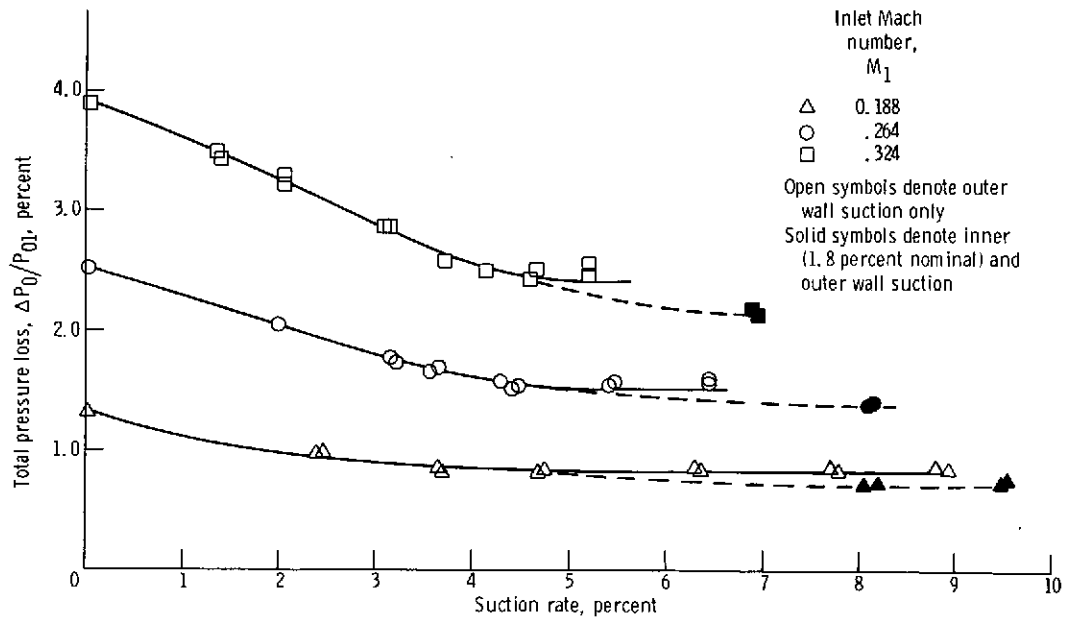
Figure 7. – Effect of suction on diffuser effectiveness.

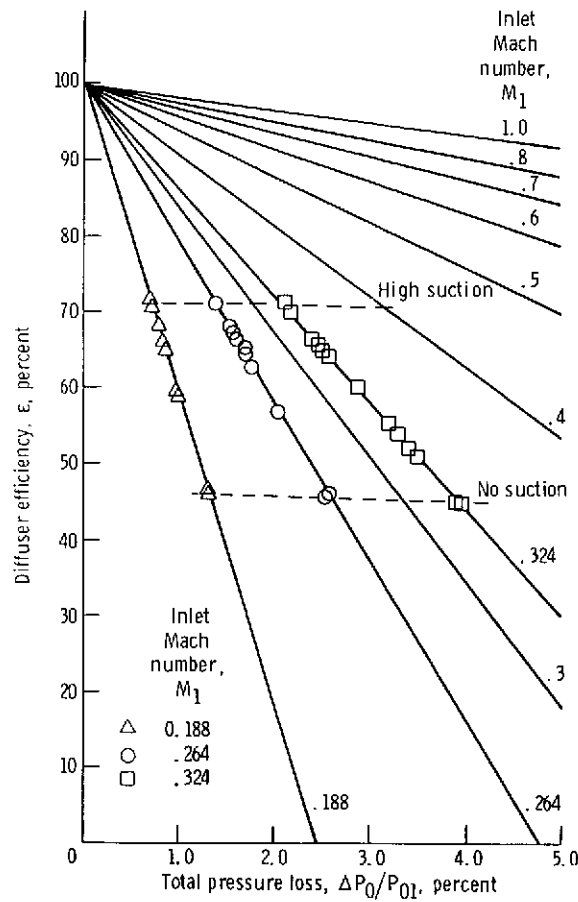Figure 8. – Effect of suction on diffuser total pressure loss.

Figure 9. - Relation between diffuser efficiency and total pressure loss with inlet Mach number as a parameter. Specific heat ratio γ = 1.4.
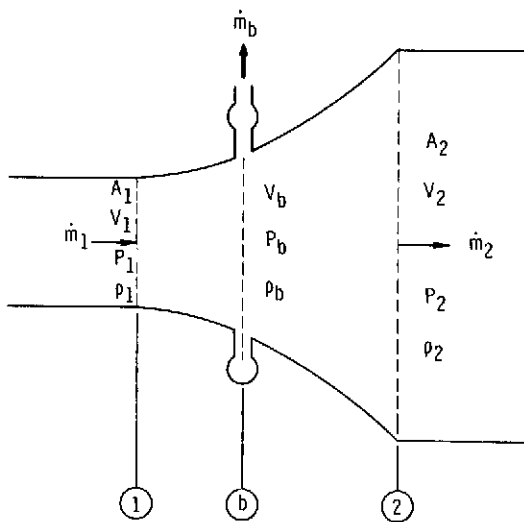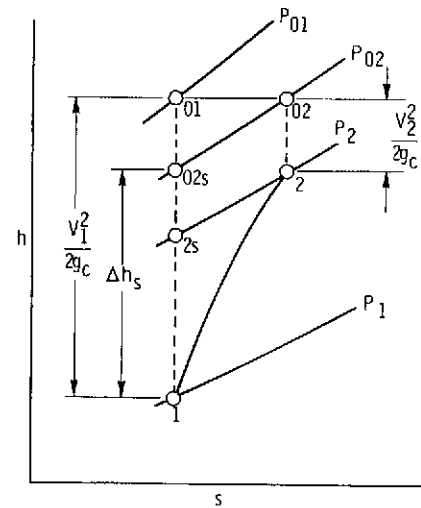

Figure 10. - Schematic diagram of diffuser with wall bleed.

Figure 11. - Diffuser enthalpy-entropy diagram.